Colon Segmentation for Prepless Virtual Colonoscopy

Vahid Taimouri, Xin Liu, Zhaoqiang Lai, Chang Liu, Darshan Pai, and Jing Hua, *Member, IEEE*

Abstract—A novel segmentation framework for a prepless virtual colonoscopy (VC) is presented, which reduces the necessity for colon cleansing before the CT scan. The patient is injected rectally with a water-soluble iodinated contrast medium using manual insufflators and a small rectal catheter. Compared to the air-based contrast medium, this technique can better preserve the color lumen and reduce the partial volume effect. However, the contrast medium, together with the fecal materials and air, makes colon wall segmentation challenging. Our solution makes no assumptions about the shape, size, and location of the fecal material in the colon. This generality allows us to label the fecal material accurately and extract the colon wall reliably. The accuracy of our technique has been verified on 60 human subjects. Compared with current VC technologies, our method is shown to be better in terms of both sensitivity and specificity. Further, in our experiments, the accuracy of the technique was comparable to that of optical colonoscopy results.

Index Terms—Colon segmentation, CT colonography (CTC), electronic colon cleansing (ECC).

I. INTRODUCTION

OPTICAL colonoscopy (OC) and CT colonography (CTC) detect colonic abnormalities such as polyps and cancerous lesions. Both techniques require a colon cleansing preparation without residual fecal materials; otherwise, residues may prevent the camera from traversing the colon in OC, or be labeled as polyps in CTC. As part of the preparation process, the colon is either washed by injecting large amounts of liquid or cleaned by medications inducing aggressive bowel movements. After the preparation, air is insufflated into the colon prior to the CT scan [1], [2]. Computer-aided diagnosis systems are usually employed to extract the colon wall and detect polyps [3].

Colon cleansing is generally uncomfortable and unpleasant for many patients, especially for elderly people. There is a pressing need for virtual colonoscopy (VC) techniques that do not require physical cleansing. Toward this end, some VC procedure requires the subject to receive small amounts of iodine or dilute barium [4] orally, administered with a low-fat and low fiber diet. This procedure tags the colonic fluid and the stool

V. Taimouri, Z. Lai, C. Liu, D. Pai, and J. Hua are with the Department of Computer Science, Wayne State University, Detroit, MI 48202 USA (e-mail: vahidtaimouri@wayne.edu; kevinlai@wayne.edu; changliu@wayne.edu; darshan@wayne.edu; jinghua@wayne.edu).

X. Liu is with the Department of Radiology, Yue Bei People's Hospital, Guangdong 512026, China (e-mail: liuxin0077007@sina.com).

Color versions of one or more of the figures in this paper are available online at http://ieeexplore.ieee.org.

remnants. These residual materials appear highly attenuated in corresponding CT images. Subsequently, fecal subtraction algorithms [5] remove stools and retain the colon surface. Although VC precludes the physical cleansing process, the diet has to begin several days before the CT scan and may be unpleasant for some persons. Electronic colon cleansing (ECC) leads to a shorter evaluation time, lower assessment effort, and greater observer confidence than CTC without electronic cleansing to obtain similar lesion conspicuity [6]. A ray-based detection algorithm [7], a gradient-based information algorithm [8], and a statistical expectation-maximization algorithm [9] are employed to address the problems related to the partial volume effects (PVE) effect. Zalis *et al.* [10] describes a combination of morphological and spatial filtering technique to address volume averaging related artifacts which affect ECC. A structured-analysis ECC scheme was developed in [11] to identify submerged colonic structures using local morphologic information. Franaszek *et al.* [12] proposes a colon segmentation algorithm based on a hierarchy of connected air and fluid regions.

Linear polyp measurement on 3-D endoluminal views is the most reliable factor for polyp measurement when compared to 2-D views [13], [14]. Pickhardt *et al.* [15] determined the detection rates, clinical stages, and short-term patient survival for all unsuspected cancers identified during screening in CTC. The performance of double-contrast barium enemas for colorectal polyp detection is investigated and compared with CTC results in [16] and [17]. The sensitivity and specificity of CTC for the detection of colorectal polyps with and without the use of ECC are measured in [18]–[20]. Gelder *et al.* [21] compare primary 2-D and 3-D methods for CTC based on polyp detection and perceptive errors.

In this paper, we describe a new method for ECC. It involves injecting a water-soluble iodinated contrast medium into the colon via the rectum such that the colon is most filled with fluid. The contrast medium visually enhances the colon interior in the CT images of the abdomen. No techniques currently available have used an iodine-enhanced contrast medium for CTC and our method is the first to introduce an algorithm for the same. In contrast to previous VC techniques, this method does not require strict pre-scan preparation for the patient. As a result, the segmentation routine becomes challenging since the algorithm needs to remove stools of different shapes and sizes for reliable polyp measurement. Conventional colon segmentation techniques fail to extract the colon wall from CT images without serious prescan preparation. Our contributions in this paper can be summarized as follows.

1) We present a new prepless VC based on iodine-enhanced contrast medium.
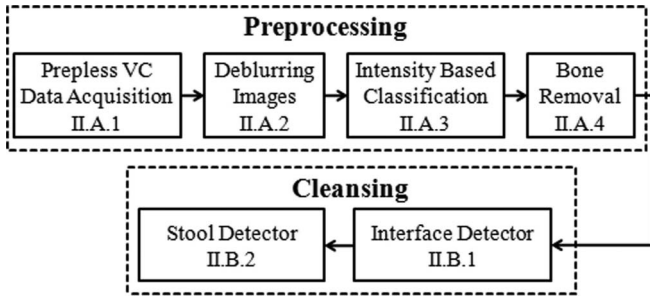2) We present an ECC pipeline to extract the colon from the CT images acquired without prescan preparation.

Fig. 1. Algorithm pipeline includes two main steps, that is, the *Preprocessing* step and the *Cleansing* step.

3) A labeling scheme is presented, which labels the various anatomical regions inside the colon.
4) A stool removal algorithm is proposed to remove stools without cutting the folds or polyps.

II. METHOD

The pipeline for segmentation is illustrated in Fig. 1. The framework is split into two stages: the *Preprocessing Stage* and the *Cleansing Stage*. During preprocessing a classification strategy is employed wherein the CT image is classified into various regions in the interior and exterior of the colon. The cleansing stage labels and cleans the colon interior in terms of stools, air, interface, or fluid. The following explains the pipeline in detail.

A. Preprocessing

1) Prepless VC Data Acquisition: In this study, we employ a new image acquisition technique in which each patient was limited to the low-fiber diet beginning one day before the scheduled morning CTC. Colonic catharsis was achieved with 250 mL 20% mannitol on the evening before the examination. Before the examination, the colon was distended with 1500 mL of water-soluble iodinated contrast medium (8 gI + /100 mL) using a manual insufflators with a small rectal catheter. Examinations were performed in supine positions on a 128-MDCT scanner (SOMATOM Definition AS, SIEMENS, Germany). The CT technique consisted of 5.00-mm collimation, 1.375 : 1 pitch, 1-mm reconstruction interval, 512×512-reconstruction array size, 120 kVp, and 50–100 mA · s. Some advantages of this imaging technique are as follows.

1) This imaging technique is more comfortable than OC and air-based VC in which some air is pumped into the colon through the rectum
2) This technique needs less preparation before image acquisition compared to other colonoscopy methods, for instance, the colon might even contain some stools which need not be removed beforehand.
3) Since iodine-enhanced contrast medium is used as the contrast agent, this technique has less PVE than the air-based colonoscopy.

2) Deblurring Images: Blurring in CT images is a major problem affecting the ability of the algorithm to detect small colonic polyps. Common sources for blurring in CT include the size of the aperture, voxel size, and the reconstruction filter. We
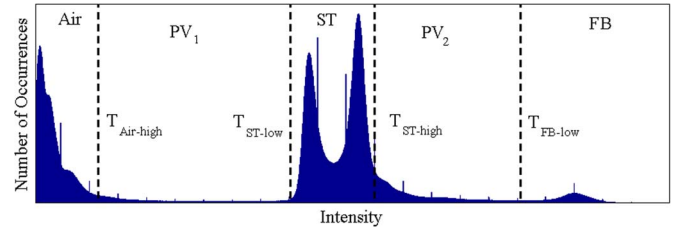

Fig. 2. Typical abdominal histogram contains different intensity regions.

use the *constrained least-squares filtering* (CLSF) to deblur the 3-D CT volume. This method is fast and only requires the mean and the variance of the noise as input. This can be calculated from the input 3-D images as follows:

$$D(u, v, k) = \left[\frac{H^*(u, v, k)}{H(u, v, k) + \gamma \left| P(u, v, k) \right|^2} \right] \quad (1)$$

where $D(u, v, k)$ is the 3-D Fourier transform of the CLFS filter, $H(u, v, k)$ is the 3-D Fourier transform of the degradation function, $H^*(u, v, k)$ is complex conjugate of $H(u, v, k)$, $P(u, v, k)$ is the 3-D Fourier transform of the Laplacian operator, and γ is an adjustable parameter.

As inferred from our experiments, we set $\gamma = 0.1$ for best results. The degradation function $H(u, v, k)$ is assumed to be a 3-D Gaussian blurring function whose kernel size depends on the spatial resolution of the input images. The size of the degradation kernel matrix is set to $5 \times 5 \times 3$. The Laplacian operator matrix is set to the same size as the degradation kernel matrix

$$\left[\begin{pmatrix} 0 & 0 & 0 \\ 0 & -1 & 0 \\ 0 & 0 & 0 \end{pmatrix}, \begin{pmatrix} 0 & -4 & 0 \\ -1 & -12 & -1 \\ 0 & -4 & 0 \end{pmatrix}, \begin{pmatrix} 0 & 0 & 0 \\ 0 & -1 & 0 \\ 0 & 0 & 0 \end{pmatrix} \right].$$

Plugging these values in (1) and multiplying the function with the input image yields a 3-D deblurred image shown as follows:

$$I_d(u, v, k) = D(u, v, k) \cdot I_b(u, v, k) \quad (2)$$

where $I_b(u, v, k)$ and $I_d(u, v, k)$ are the 3-D Fourier transforms of the blurred and deblurred images, respectively.

Standard digital signal processing techniques, such as *overlap-add* and *FFT convolution*, provide efficient methods to compute (2) in real time. In order to speed up the deblurring process and increase throughput, the input image $I_b(u, v, k)$ is broken into smaller segments and the deblurring filter is applied to each segment separately to yield the final deblurred image $I_d(u, v, k)$.

3) Intensity-Based Classification: The third step in the pipeline is to classify different anatomical regions within the CT image based on intensity values. The naming convention and classification strategy is similar to that described in [7]. The histogram and the corresponding classification of the different intensity regions are illustrated in Fig. 2. There are three main intensity regions including the *Air* region, ST (for soft tissue and stool) region, and FB (for contrast medium fluid and bone) region, which are approximately identified by defining the corresponding threshold values.

Table I represents different anatomical regions belonging to each intensity region and their corresponding color after

TABLE I
ALGORITHM LABELS VARIOUS ANATOMICAL REGIONS WITH DIFFERENT
COLORS BASED ON THEIR INTENSITIES

Anatomical Region	Intensity Region	Assigned Color
Air	Air	Red
Soft Tissue	ST	Brown
PVE and mucosa	PV_1	Pink
Fluid (Contrast Medium) [a]	FB	Blue
Bone [a]	FB	Orange
Stool	ST	Cyan
Mucosa and soft tissue	PV_2	Dark Yellow
Interface	ST	Green

[a] FB represents both the bone and the fluid.

Fig. 4. Intensity of the interface is in the ST range. (a) Flat plane interface surrounding a big air component. (b) Hemisphere interface surrounding a small air component.
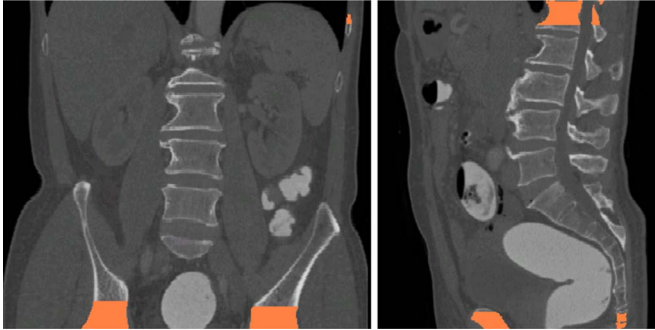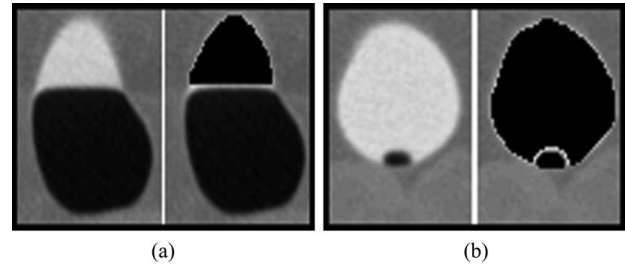
Fig. 3. *Left*: some seed voxels are selected on both sides of the pelvis. *Right*: some seed voxels are selected on both sides of the pelvis, the upper spine, and ribs.

segmentation. There are two more intensity regions PV_1 and PV_2 (for partial volumes). PV_1 region contains some PVE and mucosa voxels at the intersection of air and soft tissue, and PV_2 includes some soft tissue and mucosa voxels at the intersection of fluid and soft tissue, or between fluid and stools. Note that our algorithm does not depend on accurate determination of the thresholds. However, Due to having the same intensities, interface, stool, and soft tissue cannot be separated by the thresholds.

4) Bone Removal: As the bone intensity is in the FB range, bones might be classified by mistake as part of the colon which incurs the wrong colon segmentation and even failure of the whole pipeline. Therefore, one major task is to distinguish between bone and colon, and to eliminate bones before execution of the stool removal algorithm. Due to variety of image quality in different scanners, the bone intensity changes in images acquired by different scanners. In addition, bones have wide range of intensities.

The abdominal images contain all tissues from lower hip to middle chest, and bones are in either the spine or ribs or the pelvis, whose locations are known. In order to label the bone, some FB voxels are labeled as the bone seed voxels on both sides of the pelvis in the lower abdomen, and some on the spine or the ribs near lungs (see Fig. 3). Then, we use 26-connected neighborhood to grow the bones from the bone seed voxels to their adjacent FB voxels and to separate the bones from the fluid voxels.

B. Cleansing

Cleansing the colon is equivalent to replacing every voxel within the colon with intensities classified as air (see Fig. 10). The voxels representing the colon interior are normally within the Air, ST, and FB regions. Instead of replacing the intensities, we label the interiors based on the detection algorithm.

1) Interface Detector: Fig. 4 illustrates the problem concerning the interface between air and fluid. These intensities are normally in the ST range and can be wrongly classified as soft tissue. The right image of Fig. 4(a) shows the result when fluid intensities were replaced by air. The interface is classified as soft tissue, and isolates part of the colon, which is undesirable. Another effect of this is shown in Fig. 4 where a very small air pocket in one of the slices has been misinterpreted as a polyp in the right image of Fig. 4(b). This can reduce the sensitivity of the algorithm resulting in a high false positive rate (FPR). In order to avoid these potential issues, we detect the air–fluid interface in a two-step procedure.

1) A 3-D Sobel filter marks edges of the image. Edge voxels adjacent to both fluid and air voxels are labeled as interface. The following pseudocode illustrates this step in the vertical direction
   - a) $E \leftarrow$ 3-D Sobel Filter(V)
   - b) **for** each ST or PV_2 voxel $\in E$ **do**
   - c)   **for** ($x = 1$ to N) AND ($y = 1$ to N) **do**
   - d)   **if** ($L(x\uparrow) =$ Air) AND ($L(y\downarrow) =$ FB) **then**
   - e)   Relabel the voxel as INTERFACE
   - f)   **end if**
   - g)   **end for**
   - h) **end for**

   where V, E, and N represent input volume, edge voxels, and number of neighboring voxels being checked, respectively. $L(idx)$ is label of the voxel idx, $n \uparrow$ and $n \downarrow$ are indices of nth upward and downward adjacent voxels, respectively. Note that the same procedure is applicable to detect the interfaces in the horizontal direction.
2) PV_2 or ST voxels in the six neighborhood of interface voxels are labeled as an interface.

The first step does not label some parts of the interface where the interface connects to soft tissue, which results in some interface residues. For instance, Fig. 5 illustrates some interface residues resembling two polyps in 2-D view [see Fig. 5(a)] and a ring around the air bubble in 3-D view [see Fig. 5(b)]. The second step labels the interface residues effectively and extracts a smooth colon wall [see Fig. 8(c) and (f)]. Up until now, the interface is separated from soft tissue and stool, and colored in green.

2) Stool Detector: Labeling fecal materials is more challenging than interface detection because their shape and characteristics vary across patients depending on age, sex, health,
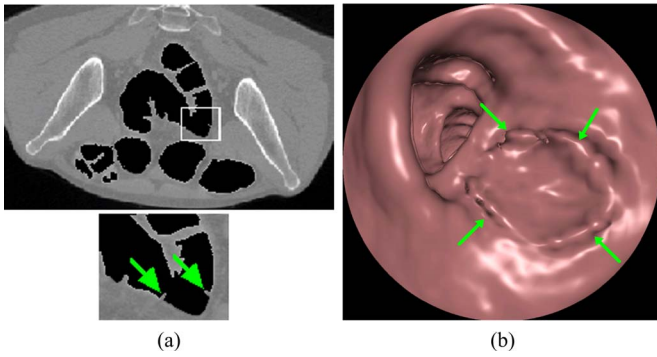
Fig. 5. (a) Interface residues near soft tissue appear like polyps in 2-D view, which leads to wrong diagnosis. (b) Undetected interface residue in 3-D view resembles a ring on the colon surface.
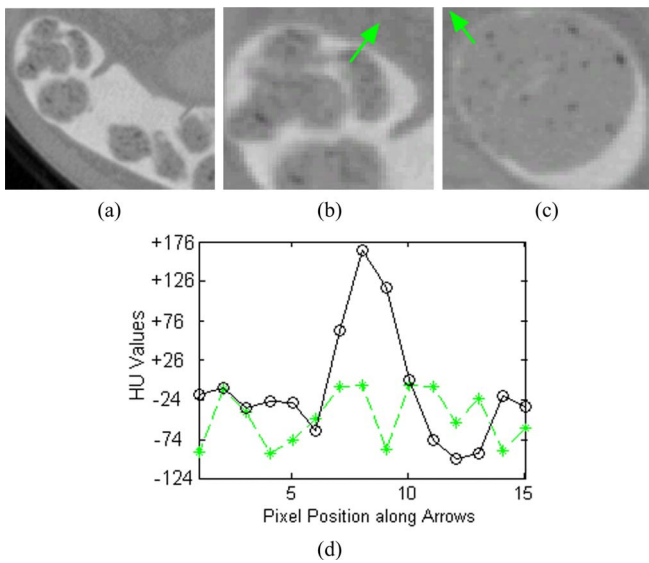

Fig. 6. (a) Attached and isolated stools in the colon are of any size and shape. (b) Small stool connects to the wall by PV_2 voxels, which is labeled in the first step. (c) Big stool attaches to the colon by ST and PV_2 voxels. (d) Solid curve with circle and the dashed curve with asterisk depict the changes of intensities along two arrows in (b) and (c), respectively.

lifestyle, etc. Moreover, changes in image acquisition parameters affect the texture of stools making localization difficult. Basically, stools are classified into two major types based on their shapes and sizes [see Fig. 6(a)]. 1) *Isolated stools*: immersed in fluid without attaching to the colon wall. 2) *Attached stools*: attached to the colon wall through some voxels, called *Connecting Voxels* (CV). Although extraction of the isolated stools can simply be carried out by a threshold filter, accurate labeling of the attached stools is more challenging since soft tissue and stools have the same intensity range as described earlier. We tackle labeling of attached stools in three steps.

a) Defining seed voxels: If an attached stool is divided into smaller pieces, most of the pieces are not attached to the wall anymore. Based on this idea, some planes are intersected with the abdominal part to divide stools into some thin layers, and then mark the isolated ST voxels as primary seed voxels (PSV). It is obvious that PSV contain neither CV nor folds since they are not isolated. We intersected axial, coronal, and sagittal planes

with the abdomen, since some stools that are not isolated from one view might become isolated from another view.

1) $I \leftarrow$ Intersection of Axial, Sagittal, and Coronal Planes with V
2) $S \leftarrow$ Find Isolated ST or PV_2 Components $\in I$
3) Relabel S as PSV.

In contrast with small stools Fig. 6(b), big stools are likely to attach to the wall from all the directions Fig. 6(c) incurring the failure of the intersecting planes to mark PSV effectively. This in turn makes execution of the next step crucial.

b) Labeling attached stool components: As mentioned, attached stools connect to the colon wall by some CV. The CV of small stools contain only PV_2 voxels, yet CV of big stools contain both ST and PV_2 voxels. For instance, intensities of voxels along the arrows in Fig. 6(b) and (c) are shown in Fig. 6(d). As seen, for small stools intensity changes noticeably near the wall (solid line with circle), yet it does not change for big stools (dash line with asterisk). In this situation, the first step fails to mark big stools, since their CV contains ST voxels, and the stool layers are not isolated anymore. To handle this problem, we relabel the ST voxels of CV to PV_2, and execute the first step again, but at this point the seed voxels are called secondary seed voxels (SSV).

1) **for** (each PV_2 voxel idx) AND (each ST voxel $\in N_6(idx)$) **do**
2)   Relabel the ST voxel as PV_2
3) **end for**
4) Relabel all PV_2 voxels as FLUID
5) Execute the first step again and label SSV

where $N_6(idx)$ represents six neighborhood of the voxel idx.

c) Smoothing operation: Finally, PSV, SSV, and ST or PV_2 voxels in their neighborhood are marked as stool. The number of neighboring voxels highly depends on the amount and size of stools. However, this step should be carried out with caution; otherwise, some parts of the colon wall or folds might be marked as stool. According to our experiences, six neighborhood yields the best results in terms of having the best FPR.

In contrast with polyps, stool components usually contain low or high intensity voxels, which is used as a differentiating criterion to avoid mislabeling polyps as stool, and lower false negative rate. Therefore, we examine the textures of labeled components to verify the segmentation. This problem is described more in Section IV. However, if the verification method cannot assure whether a labeled component is a polyp with a high certainty, we label it as a suspicious component, not as stool, so that physicians can investigate more by VC navigation. Therefore, no polyp will be overlooked and the confidence rate of the procedure would increase considerably.

III. EXPERIMENTAL RESULTS

In total, 60 scans from human subjects were acquired according to the protocol described earlier. Each scan contains 450 images in average. For some subjects both supine and prone scans were acquired, but the others were only scanned in supine position. Some datasets have cancerous or polypoid lesions whose sizes and positions were documented by OC reports or verified by radiologists.
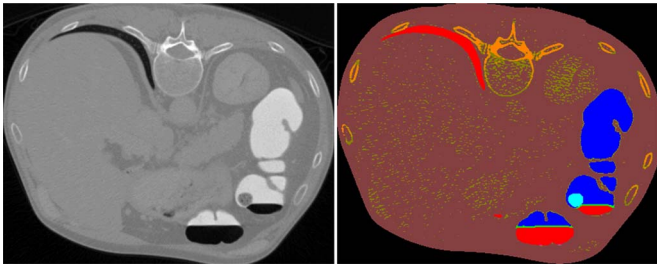
Fig. 7. Axial slice shows the lower part of the left lung along with some fluid, air, and stool inside the colon, which are segmented by the algorithm and assigned different colors as in Table I.
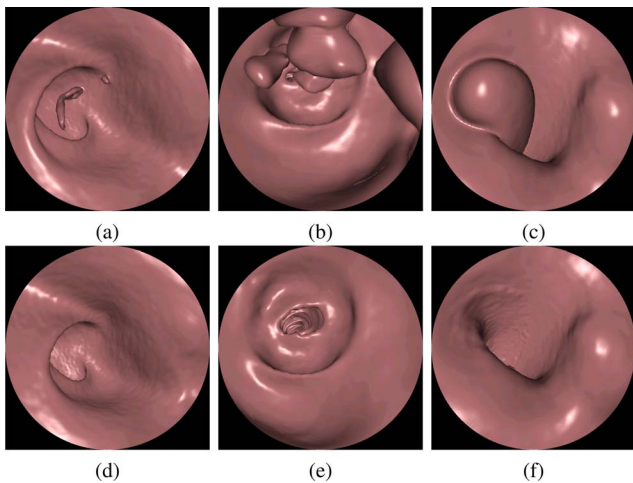

Fig. 8. (a)Small attached stool. (b) Some attached stools with different sizes. (c) Big air component. (d)–(f) After cleansing the colon, the colon surface is extracted precisely. As seen in (c) and (f), after removing air bubble there is no interface residue of ring shape around the air bubble.

To verify performance of our algorithm, a multithreaded C++ application in windows vista 64 bit environment was implemented. We have plugged our software tool into the Yulonn Virtual Colonoscopy software platform provided by the Yulonn Medical Imaging Company, Ltd. In average the program takes about 3 min to extract the colon surface for virtual flying through on a Pentium PC with 3 GHz CPU speed and 4-GB RAM memory. Fig. 7 depicts an axial slice and the colors assigned to each anatomical region as in Table I.

The physician can virtually fly through the extracted colon surface and see any polyp or cancerous lesion (see Fig. 8) with the Yulonn Virtual Colonoscopy software system. As represented in Fig. 8(a)–(c), some stool and air components of different sizes have clogged the colon. The algorithm can successfully remove them to achieve a smooth surface [see Fig. 8(d)–(f)]. It is notable that the air component was detected and removed without any ring-shaped residues [see Fig. 8(c) and (f)].

Two experienced radiologists evaluated the performance of our method using both 2-D CT images and 3-D fly through. The subjectivity is eliminated by cross checking between the radiologists. In the first step, the radiologists used the 3-D fly through to see the colon interior as in OC; once, they encounter a suspicious lesion, they click on it to find its corresponding location on the 2-D slices, and confirm that if it is a real polyp

TABLE II
SENSITIVITY AND SPECIFICITY OF THE ALGORITHM

Polyp Size(mm)	Sensitivity(%)	Specificity(%)	p value
$5mm - 10mm$	92.35	91.02	0.05
$\geq 10mm$	96.27	95.12	0.05

or not. In the second step, they first spot polyps on the 2-D slices, and then click on each polyp to see it on the 3-D fly through, and make sure that the polyp is not wrongly removed in the 3-D extracted colon.

Sensitivity and specificity in detecting different colonic polyps is as shown in Table II. We mainly focus on the polyps bigger than 5 mm which are clinically more important. The sensitivity reported in [18] for the detection of polyps of 5–10 mm and $\geq$10 mm was 72.9% and 83.3%, respectively, and in [22], the sensitivity for polypoid adenomas and all polypoid lesions of $\geq$6 mm was 86.2% and 81.0%, respectively. Furthermore, the sensitivity and specificity per patient in [18] were 91% and 86%, respectively. As seen, the sensitivity and specificity of this prepless method are as admissible as other ECC methods which need preparation before CTC.

After labeling the seed voxels, texture of the labeled components are examined to avoid any mislabeling. Fig. 9 depicts some polyps and cancerous lesions detected by our method and their corresponding OC results. The polyps are of different sizes and located in different parts of the colon. As seen, the polyps and the cancerous lesions are extracted without being cut out or split into pieces by the algorithm.

Fig. 10(a) and (b) shows 2-D view of some big attached stools in the colon before and after cleansing, and Fig. 10(c) and (d) depicts 2-D view of some small stools before and after cleansing, respectively. As seen, although some stools are nearby air and the others are attached to the wall or folds, the algorithm can cleanse the colon without cutting any fold. Fig. 10(e) and (f) shows 2-D view of some air bubbles of different sizes before and after the cleansing. The algorithm can detect the interfaces completely without leaving any bumpy-shaped residue nearby soft tissue. Also in Fig. 10(e) and (f), two arrows point to a polyp detected in the air bubble before and after cleansing.

IV. DISCUSSION AND CONCLUSION

The proposed algorithm can segment and extract the colon without the need of any preparation beforehand. The algorithm does not have any presumption about size, shape, and location of air and stool components inside the colon, whereas it uses the colon shape to intersect some planes with the abdominal volume, and label the colon. The verification results confirm the effectiveness of the algorithm to segment different datasets with different amounts of stools, air, and contrast agent fluid within few minutes. Overall, the proposed pipeline has a great potential for clinical VC.

A useful characteristic of the algorithm is the independence of the first and second steps of the stool detector algorithm, that is, depending on the amount of stool in the colon, only the first step or both steps are executed, which speeds up the algorithm execution on roughly clean datasets having little amount of
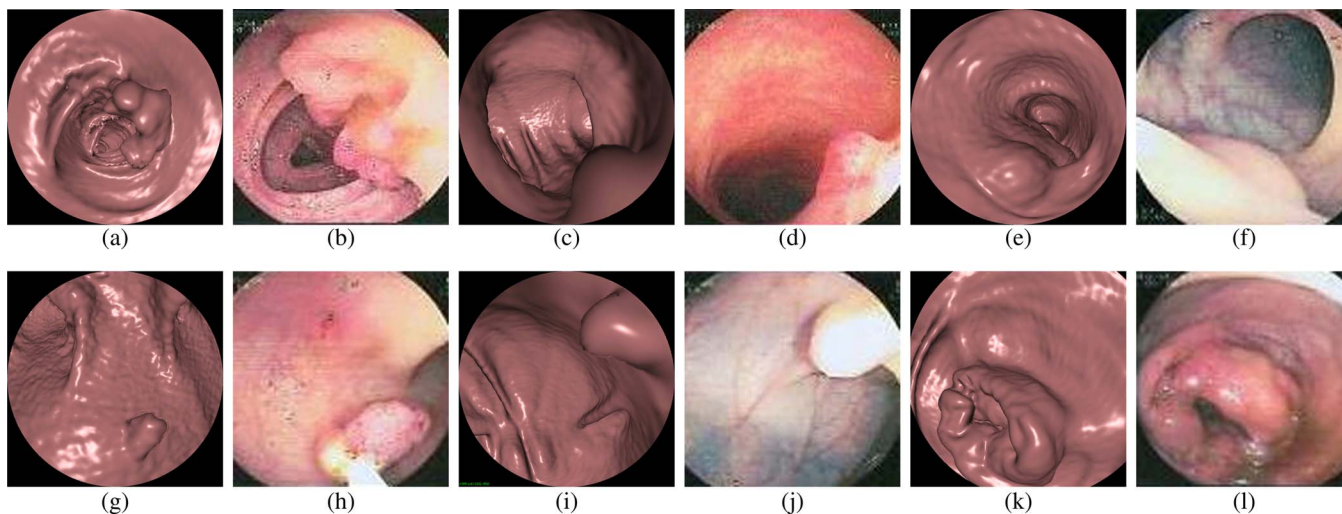
Fig. 9. First, third, and fifth columns represent VC images of some polyps and cancer lesions; the second, fourth, and sixth columns depict their corresponding OC images. (a) and (b) Polyp of size 35 mm × 20 mm in the sigmoid colon. (c) and (d) Polyp of size 5 mm in the rectum. (e) and (f) Suspicious lesion of size 85 mm × 20 mm in the rectum. (g) and (h) Hemisphere polyp of size 18 mm × 18 mm × 15 mm in the rectum. (i) and (j) Polyp of size 10 mm in the ascending colon. (k) and (l) Cauliflower shape cancerous lesion in the ascending colon.
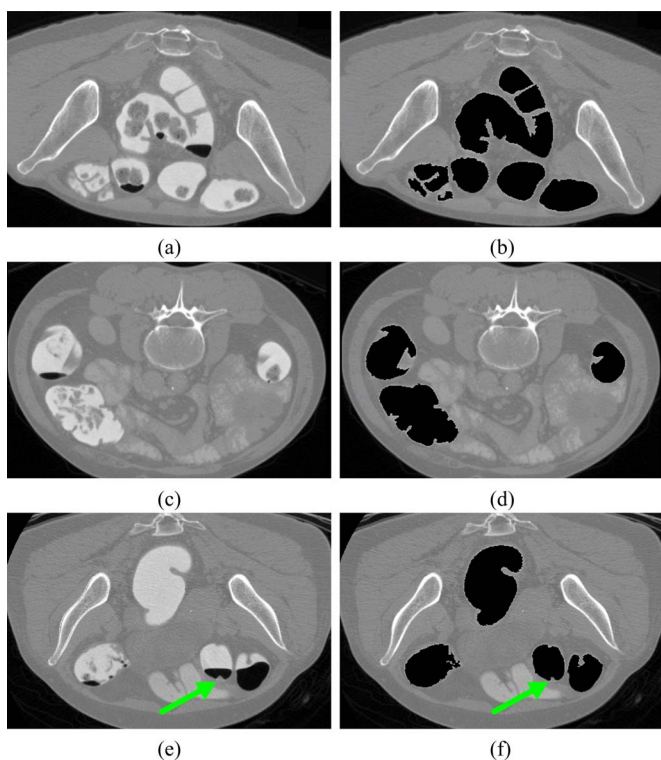

Fig. 10. Some slices before and after cleansing the colon on the left and right columns, respectively. (a) and (b) Some big stools attach to the folds or air components. (c) and (d) Some small stools are either isolated or attached to the wall. (e) and (f) Polyp inside the air bubble is pointed by the arrow.
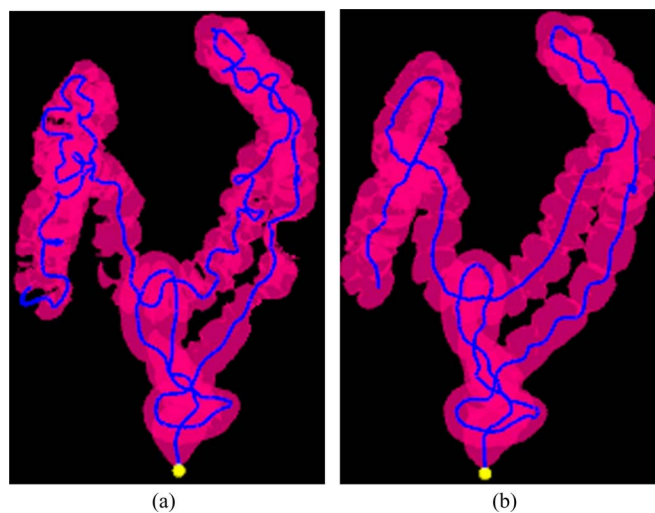

Fig. 11. (a) Due to existence of stools of different sizes in different locations inside the colon, the colon might be partially or completely clogged by stools, which results in the center line being distorted; therefore, the user may feel as if the virtual camera trembles as it flies through the colon, which is disturbing the user, and even may obstruct the diagnostic process. (b) By contrast, the center line of the cleansed colon is determined precisely everywhere along the colon so that the virtual camera can fly through the colon smoothly.

stools accordingly. In other words, since the second step is to label big stools which are not labeled in the first step, if there is a small amount of stool in the colon, the first step can label the stools completely; therefore, the execution of the second step can be avoided without loss of efficiency.

The VC application uses the center line of the colon as the path to fly through and show the inside of the colon. But big stools may block the colon such that the center line is disrupted, or may distort the center line, either of the cases, the camera cannot fly through easily which results in inaccurate recognition of polyps or cancerous lesions. In all the datasets, the center line was distorted by stools before cleansing, and in eight of them, the center line was disrupted at some points. Nonetheless, after cleansing, the center line was determined completely without disruption (see Fig. 11).

Due to the injection of different amount of fluid before image acquisition, some fluid may overflow into the small intestine causing both the small intestine and colon being labeled as fluid [see Fig. 12(a)]. Being separated from the small intestine, stools
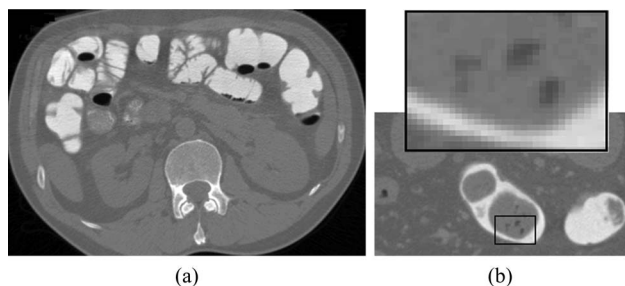
Fig. 12. (a) Contrast agent fluid overflows into the small intestine, thus its intensity would be in the FB range. (b) Low intensity voxels are inside the stools of size (≥ 5 mm) is an advantageous measure to discriminate them from polyps.

inside the colon can still be labeled by the intersecting planes, thus fluid overflow into the small intestine has no performance impact which needs to be elaborated.

As aforementioned, stools are of any shape and size. According to our experiences, most of stools smaller than 5 mm are fully tagged by the contrast agent fluid and can be distinguished from the polyps by applying a threshold filter. But if they are not completely tagged, they can be detected based on their shape [9]. By contrast, most of stool bigger than 5 mm are not completely tagged and can be of any shape; therefore, both threshold and shape-based filters fail to recognize them from polyps. As shown in Fig. 12(b), in contrast with polyps, most of big stools contain some low or high intensity voxels, thus texture-based techniques can differentiate them. After labeling components by the algorithm, the histograms of the labeled components are used to confirm the labeled components and avoid wrong labeling of polyps as stool, which lowers the false negative rate.

However, if the polyp is completely surrounded by stools attaching to it, growing the stool region to the neighborhood may label the polyp as stool. As a result, a polyp may be partially or completely removed depending on the polyp size. Nevertheless, if the attached stools change the locations in the supine and prone scans, the stools can be marked correctly without affecting the polyps by comparison of the two positions [23]. The small stools whose locations are fixed might be accurately checked in terms shape and texture to avoid any mislabeling. This part will be further investigated in the future work.

ACKNOWLEDGMENT

REFERENCES

[1] P. Lefere, S. Gryspeerdt, J. Dewyspelaere, M. Baekelandt, and B. Van Holsbeeck, "Dietary fecal tagging as a cleansing method before CT colonography: Initial results polyp detection and patient acceptance," *Radiology*, vol. 224, pp. 393–403, 2002.
[2] S. Mahgerefteh, S. Fraifeld, A. Blachar, and J. Sosna, "CT colonography with decreased purgation: Balancing preparation, performance, and patient acceptance," *Amer. J. Roentgenol.*, vol. 193, pp. 1531–1539, 2009.
[3] R. M. Summers, M. Franaszek, M. T. Miller, P. J. Pickhardt, J. R. Choi, and W. R. Schindler, "Computer-aided detection of polyps on oral contrast-enhanced CT colonography," *Amer. J. Roentgenol.*, vol. 184, pp. 105–108, 2005.
[4] P. J. Pickhardt and J. R. Choi, "Electronic cleansing and stool tagging in CT colonography: Advantages and pitfalls with primary three-dimensional evaluation," *Amer. J. Roentgenol.*, vol. 181, pp. 799–805, 2003.
[5] M. Zalis and P. Hahn, "Digital subtraction bowel cleansing in CT colonography," *Amer. J. Roentgenol.*, vol. 176, pp. 646–648, 2001.
[6] I. W. O. Serlie, A. H. de Vries, L. J. van Vliet, C. Y. Nio, R. Truyen, J. Stoker, and F. M. Vos, "Lesion conspicuity and efficiency of CT colonography with electronic cleansing based on a three-material transition model," *Amer. J. Roentgenol.*, vol. 191, pp. 1493–1502, 2008.
[7] S. Lakare, M. Wan, M. Sato, and A. Kaufman, "3D digital cleansing using segmentation rays," in *Proc. IEEE Vis. Conf.*, 2000, pp. 37–44.
[8] D. Chen, Z. Liang, M. R. Wax, L. Li, B. Li, and A. E. Kaufman, "A novel approach to extract Colon Lumen from CT images for virtual colonoscopy," *IEEE Trans. Med. Imag.*, vol. 19, no. 12, pp. 1220–1226, Dec. 2000.
[9] Z. Wang, Z. Liang, X. Li, D. Eremina, and H. Lu, "An improved electronic colon cleansing method for detection of colonic polyps by virtual colonoscopy," *IEEE Trans Biomed. Eng.*, vol. 53, no. 8, pp. 1635–1646, Aug. 2006.
[10] M. Zalis, J. Perumpillichira, and P. Hahn, "Digital subtraction bowel cleansing for CT colonography using morphological and linear filtration methods," *IEEE Trans. Med. Imag.*, vol. 23, no. 11, pp. 1335–1343, Nov. 2004.
[11] W. Cai, H. Yoshida, M. E. Zalis, J. J. Nappi, and G. J. Harris, "Informatics in radiology: Electronic cleansing for non-cathartic CT colonography: A structure-analysis scheme," *RadioGraphics*, vol. 30, pp. 585–602, 2010.
[12] M. Franaszek, R. M. Summers, P. J. Pickhardt, and J. R. Choi, "Hybrid segmentation of colon filled with air and opacified fluid for CT colonography," *IEEE Trans. Med. Imag.*, vol. 25, no. 3, pp. 358–368, Mar. 2006.
[13] P. J. Pickhardt, A. D. Lee, E. G. McFarland, and A. J. Taylor, "Linear polyp measurement at CT colonography: *In vitro* and *in vivo* comparison of two-dimensional and three-dimensional displays," *Radiology*, vol. 236, pp. 872–878, 2005.
[14] E. Bethea, O. K. Nwawka, and A. H. Dachman, "Comparison of polyp size and volume at CT colonography: Implications for follow-up CT colonography," *Amer. J. Roentgenol*, vol. 193, pp. 1561–1567, 2009.
[15] P. J. Pickhardt, D. H. Kim, R. J. Meiners, K. S. Wyatt, M. E. Hanson, D. S. Barlow, P. A. Cullen, R. A. Remtulla, and B. D. Cash, "Colorectal and extracolonic cancers detected at screening CT colonography in 10286 asymptomatic adults," *Radiology*, vol. 255, pp. 83–88, 2010.
[16] J. T. Ferrucci, "Double-contrast barium enema: Use in practice and implications for CT colonography," *Amer. J. Roentgenol.*, vol. 187, pp. 170–173, 2006.
[17] J. Sosna, T. Sella, O. Sy, P. T. Lavin, R. Eliahou, S. Fraifeld, and E. Libson, "Critical analysis of the performance of double-contrast barium enema for detecting colorectal polyps ≥ 6 mm in the era of CT colonography," *Amer. J. Roentgenol.*, vol. 190, pp. 374–385, 2008.
[18] M. S. Juchems, A. Ernst, P. Johnson, S. Virmani, H. J. Brambs, and A. J. Aschoff, "Electronic colon-cleansing for CT colonography: Diagnostic performance," *Abdom. Imag.*, vol. 34, pp. 359–364, 2009.
[19] S. H. Park, S. Kim, S. Lee, L. Bogoni, A. Kim, S. Yang, S. Myung, J. Byeon, B. Ye, and H. Ha, "Sensitivity of CT colonography for nonpolypoid colorectal lesions interpreted by human readers and with computer-aided detection," *Amer. J. Roentgenol.*, vol. 193, pp. 70–78, 2009.
[20] P. Pickhardt, J. Choi, I. Hwang, J. Butler, M. Puckett, H. Hildebrandt, R. Wong, P. Nugent, P. Mysliwiec, and W. Schindler, "Computed tomographic virtual colonoscopy to screen for colorectal neoplasia in asymptomatic adults," *N. Engl. J. Med.*, vol. 349, pp. 2191–2200, 2003.
[21] R. E. van Gelder, J. Florie, C. Nio, S. Jensch, S. de Jager, F. Vos, H. Venema, J. Bartelsman, P. Reitsma, P. Bossuyt, J. Lamris, and J. Stoker, "A comparison of primary two and three dimensional methods to review CT colonography," *Eur. Radiol.*, vol. 17, pp. 1181–1192, 2007.
[22] P. Pickhardt, P. Nugent, J. Choi, and W. Schindler, "Flat colorectal lesions in asymptomatic adults: Implications for screening with CT virtual colonoscopy," *Amer. J. Roentgenol.*, vol. 183, pp. 1343–1347, 2004.
[23] Z. Lai, J. Hu, C. Liu, V. Taimouri, D. Pai, J. Zhu, J. Xu, and J. Hua, "Intra-patient supine-prone colon registration in CT colonography using shape spectrum," in *Proc. 13th Int. Conf. Med. Image Comput. Comput. Assist. Intervent.*, 2010, pp. 332–339.

Authors' photographs and biographies not available at the time of publication.